J Electr Eng Technol.2018; 13(3): 1265-1274
http://doi.org/10.5370/JEET.2018.13.3.1265

ISSN(Print) 1975-0102
ISSN(Online) 2093-7423

Virtual Flux and Positive-Sequence Power Based Control of Grid-Interfaced Converters Against Unbalanced and Distorted Grid Conditions

Yukun Tao* and Wenhu Tang†

Abstract – This paper proposes a virtual flux (VF) and positive-sequence power based control strategy to improve the performance of grid-interfaced three-phase voltage source converters against unbalanced and distorted grid conditions. By using a second-order generalized integrator (SOGI) based VF observer, the proposed strategy achieves an AC voltage sensorless and grid frequency adaptive control. Aiming to realize a balanced sinusoidal line current operation, the fundamental positive-sequence component based instantaneous power is utilized as the control variable. Moreover, the fundamental negative-sequence VF feedforward and the harmonic attenuation ability of a sequence component generator are employed to further enhance the unbalance regulation ability and the harmonic tolerance of line currents, respectively. Finally, the proposed scheme is completed by combining the foregoing two elements with a predictive direct power control (PDPC). In order to verify the feasibility and validity of the proposed SOGI-VFPDPC, the scenarios of unbalanced voltage dip, higher harmonic distortion and grid frequency deviation are investigated in simulation and experimental studies. The corresponding results demonstrate that the proposed strategy ensures a balanced sinusoidal line current operation with excellent steady-state and transient behaviors under general grid conditions.

Keywords: Voltage sensorless control, Virtual flux (VF), Positive-sequence power, Grid-interfaced converter, Fault tolerance.

1. Introduction

Recently, as a high-performance power interface, voltage source converters (VSCs) have been widely used in electric power systems. For adjustable speed drives with power regeneration [1], one of the most conventional applications, such a converter mainly operates at the rectifier mode. On the contrary, the inverter mode of VSCs is primary in renewable energy integrations (e.g. wind turbine, photovoltaic) [2], which are burgeoning fields for VSC applications.

In order to adapt to the application development of grid-interactive VSCs, the fault-ride-through capability of which should be expected by future control strategies [3, 4]. To meet this requirement, two important types can be identified from the traditional control strategies: voltage oriented control (VOC) [5] and direct power control (DPC) [6, 7]. The line current and the instantaneous power are utilized as control variables in the former and the latter, respectively. From the published works it can be found that the ideal grid voltage waveforms are usually the base for control strategy derivation and experimental verification, such as the ones developed in [8, 9]. Nevertheless, this ideal assumption may degenerate controller performance caused by nonideal cases. Even if numerous control strategies have been proposed to cope with nonideal grid conditions, balanced sinusoidal line currents cannot be realized when the active power or reactive power operates at a constant value [10, 11]. Under a seriously distorted and unbalanced grid condition, the constant active power and reactive power also cannot be obtained at the same time. It means that only one of the requirements mentioned above can be met at a time, and this paper concentrates on the balanced sinusoidal current operation.

In the published DPCs, the fluctuating power compensation method is a main way to deal with grid disturbances [11, 12]. Following this method, extractions of sequence components are inevitable. However, the harmonic extractions would increase the calculation burden of control hardware processers when higher harmonics are contained in grid voltages. As exceptions, in [13], additional calculations, i.e. a low pass filter (LPF) and a phase lock loop, were introduced to compensate for the imbalanced line voltage condition. As a result, the effect is not satisfactory. In [14], the negative-sequence grid voltage was extracted and added to the reference voltage of VSC, whereas the sequence estimator used the Park and inverse

† Corresponding Author: School of Electric Power Engineering, South China University of Technology, Guangzhou, China. (wenhutang@scut.edu.cn)
* School of Electrical and Information Engineering, Zhengzhou University of Light Industry, Zhengzhou, China. (taoyk@zzuli.edu.cn)
Received: May 22, 2017; Accepted: January 26, 2018

Park transformations in addition to a LPF and a notch filter. That means the estimating process would slow down the transient response of the controller. Although the strategy proposed in [15] was only based on the positive sequence detection, the design rules of which was complicated. The published literatures also indicate that only unbalanced grid voltage dips are concerned in most cases for grid disturbances. In terms of higher harmonic disturbances, [14] utilized auxiliary harmonic compensators, which were added to the primary controller. With the concerned harmonics increasing, the processer burden would be heavier. In [9, 13], the low pass behavior of virtual flux (VF) observer was employed to improve the harmonic tolerance.

Virtual flux based schemes are popular in voltage sensorless controller designs for the following two reasons. The application of VF keeps the common advantages of sensorless strategies, such as cost reduction, reliability and generality improvements. Meanwhile, it eliminates the limitation of the orientation point for a control system [16] and enhances the harmonic tolerance [9]. The most common VF observer is designed based on a first-order LPF, however, it cannot emulate a pure integrator accurately. Later, some varieties of it were proposed to overcome this shortcoming [17, 18]. However, the above-mentioned observers are all sensitive to the grid frequency deviation. Literature [19] proposed a frequency-adaptive observer, whose behavior can be adjusted in real time according to the actual grid frequency.

In this paper, relying on the positive-sequence power and quadrature VF observer (QVFO) applications, an AC voltage sensorless and grid frequency adaptive control is proposed for grid-interfaced three-phase VSCs. This control strategy guarantees a balanced sinusoidal current operation under general grid conditions. Multiple grid disturbances, including unbalance voltage dip, grid frequency deviation and higher harmonic distortion, are considered in simulation and experimental verifications. The rest of this paper is organized as follows. Section 2 introduces a frequency-adaptive VF observer, and followed by the sequence component generation of grid VF and the mathematical model establishment for the controller. In Section 3 and 4, simulation and experimental results are presented, respectively. Finally, conclusions are drawn in Section 5.

2. Principles of the Proposed Strategy

The schematic of the proposed strategy is presented in Fig. 1, which mainly consists of the Clarke transformation (defined by (1)), frequency-adaptive VF estimation, positive- and negative-sequence component calculations (PNSC), instantaneous power estimation, converter terminal voltage reference generation and space vector modulation (SVM). The generation method for the active power reference p^*

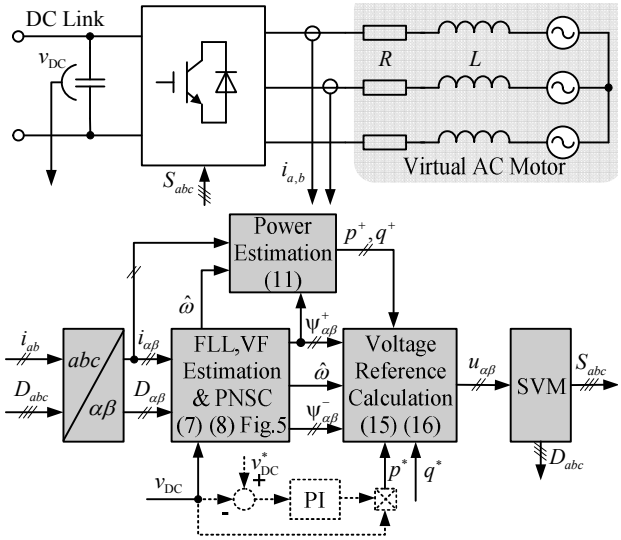

Fig. 1. Block diagram of the proposed strategy for three-phase voltage source converters

is determined by specific applications, and the component drawn with dashed lines in Fig. 1 shows a classic one for active front-end rectifiers.

$$T_{\alpha\beta}^{abc} = \sqrt{\frac{2}{3}}\begin{bmatrix} 1 & -\frac{1}{2} & -\frac{1}{2} \\ 0 & \frac{\sqrt{3}}{2} & -\frac{\sqrt{3}}{2} \end{bmatrix} \tag{1}$$

As revealed by Fig. 1, the proposed control strategy is established based on the estimated grid VF rather than the measured grid voltage, i.e., the proposed strategy is AC voltage sensorless.

2.1 Frequency-adaptive VF observer

The grid voltage in combination with interconnected reactors behaves as a virtual AC motor shown in Fig. 1. Then, the grid voltage can be regarded as the derivative of grid VF. Therefore, the line voltage vector $\boldsymbol{v}$ and the grid VF vector $\boldsymbol{\Psi}$ can be related by

$$\boldsymbol{\Psi} = \int \boldsymbol{v}dt + \Psi_0 \tag{2}$$

where Ψ_0 is the initial value of the flux integral. For a smooth starting process of VSCs, the initial integral value should be set correctly. Nevertheless, it is beyond the scope of this paper to discuss the initialization of VF estimation.

In this research, a frequency-adaptive QVFO (shown in Fig. 2) is developed to realize the integral action in (2), which is based on a second-order generalized integrator (SOGI). As indicated in Fig. 2, the estimated grid frequency $\hat{\omega}$ is an explicit input, which can ensure the grid frequency-adaptive performance. There is another output y of this observer in addition to Ψ. The transfer

Table 1. Frequency-domain characteristics presented at 50 Hz

L,φ	$1/s$	G_1	G_3
$L(G)$	-49.94	-49.94	-49.99
$\varphi(G)$	-90	-90	-84.29

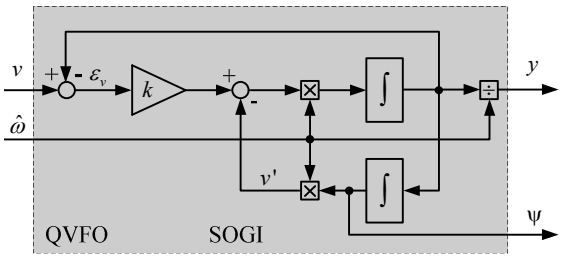

Fig. 2. Block diagram of the proposed strategy for three-phase voltage source converters

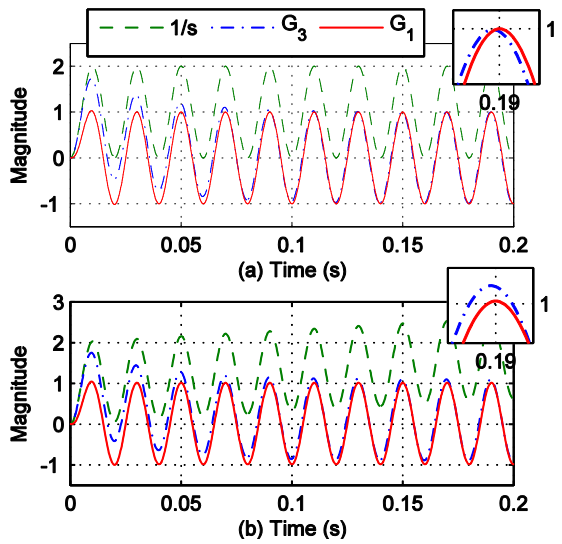

Fig. 3. Time-domain responses of G_1, G_3 and $1/s$

functions for these two signals are given by

$$G_1(s)=\frac{\Psi(s)}{v(s)}=\frac{k\hat{\omega}}{s^2+k\hat{\omega}s+\hat{\omega}^2} \tag{3}$$

$$G_2(s)=\frac{y(s)}{v(s)}=\frac{ks}{s^2+k\hat{\omega}s+\hat{\omega}^2} \tag{4}$$

where k denotes damping factor, which shapes the frequency and time-domain responses of a QVFO. Among the values of k, $\sqrt{2}$ is a good compromise between stabilization time and overshoot.

Table 1 shows the frequency-domain characteristics of the VF observers used for comparative study operating at the fundamental frequency, where $L(G)=20\lg|G|$ dB, $\varphi(G)=\angle G$ deg, and the most common VF observer, defined by $G_3(s)=1/(s+\omega_c)$ with $\omega_c=10\pi$ rad/s, is

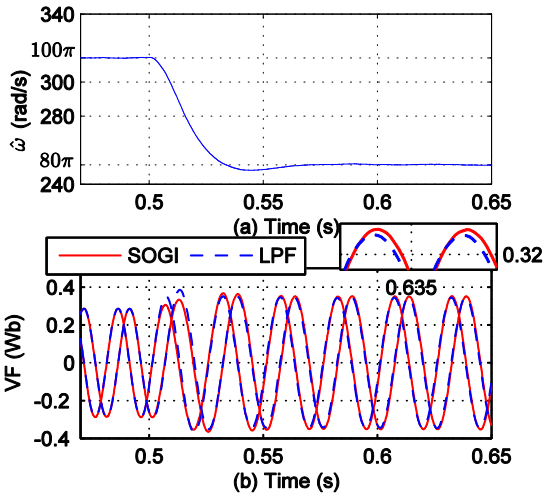

Fig. 4. Performance contrast between SOGI-based and filter-based VF observers

also given. From Table 1 it can be noted that the filter-based observer (marked by G_3) cannot emulate the pure integrator accurately at the fundamental frequency, while the SOGI-based observer offers the same amplitude and phase characters as that of $1/s$. In order to show the VF estimation results more effectively, Fig. 3 shows the time-domain response curves. The input signal for Figs. 3(a) and 3(b) are $100\pi\sin(100\pi t)$ and $3.14+100\pi\sin(100\pi t)$ (i.e. 1% DC offset included in the input signal), respectively. Fig. 3 exhibits the DC bias and integration drift problems of the pure integrator, magnitude and phase errors introduced by G_3, and the fast and accurate VF estimation offered by the SOGI-based observer independent from the interference existing in input signals.

Fig. 4 gives the simulation results for VF estimation using the SOGI-based observer and a LPF-based observer (an improved version of G_3 proposed in [17]) when the grid frequency steps from 50 to 40 Hz (the grid voltage is sinusoidal and balanced in this case). As presented in Fig. 4(b), when the grid frequency is at the rated value, i.e. 50 Hz, both observers can realize accurate estimation. Nevertheless, after the step occurrence, the LPF-based scheme introduces phase and amplitude errors, while the SOGI-based performance is not deteriorated. In other words, the frequency adaptivity of the SOGI-based observer is verified. The method for grid frequency estimation (shown in Fig. 4(a)) will be introduced in the next subsection.

2.2 Sequence component generation of the grid VF

In the $\alpha-\beta$ reference frame, the equations for the positive- and negative-sequence VF generation are

$$\begin{bmatrix}\Psi_\alpha^{+n}\\ \Psi_\beta^{+n}\end{bmatrix}=\frac{1}{2}\begin{bmatrix}1 & -q\\ q & 1\end{bmatrix}\begin{bmatrix}\Psi_\alpha^{n}\\ \Psi_\beta^{n}\end{bmatrix} \tag{5}$$

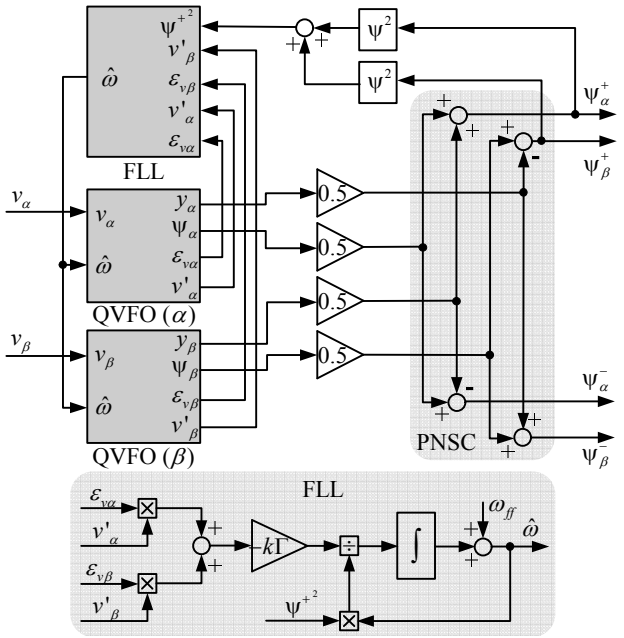

Fig. 5. Schematic of the fundamental positive- and negative-sequence VF generation by using the QVFO and a FLL

$$\begin{bmatrix} \Psi_{\alpha}^{-n} \\ \Psi_{\beta}^{-n} \end{bmatrix} = \frac{1}{2}\begin{bmatrix} 1 & q \\ -q & 1 \end{bmatrix}\begin{bmatrix} \Psi_{\alpha}^{n} \\ \Psi_{\beta}^{n} \end{bmatrix} \tag{6}$$

where the subscripts "+" and "-" represent positive- and negative-sequence components, respectively, n indicates the harmonic order, and q is defined as $e^{-j\frac{\pi}{2}}$, which generates a 90-degrees-lag phase shift of the original waveform in the time-domain.

Eqs. (5) and (6) indicate that an accurate quadrature signal generation is a necessary condition for the sequence component generation. While from (3) and (4) it is not difficult to find that the output signals y, Ψ of QVFO have the same amplitude and 90-degrees phase shift when the input signal operates at $\hat{\omega}$. Therefore, it is convenient to establish a sequence component extraction scheme based on the observer shown in Fig. 2. Aiming to achieve a frequency adaptive operation, the real-time grid frequency is required. In the literature published, there are several strategies which can meet this demand, such as the phase-locked loops (PLLs) and the frequency-locked loops (FLLs), and we adopt a type of FLL scheme here. The resulting structure for the fundamental sequence component extraction of VF is shown in Fig. 5. The aforementioned generation strategy has less computational burden and transient response time compared with the strategy involving filter based VF estimation cascaded with filter based sequence separation. Fig. 6 gives the frequency response of the transfer function from v_{α} to Ψ_{α}^{+} for both positive and negative frequency components of v_{α}. As shown in Fig. 6, the sequence component generation strategy has a higher harmonic attenuation effect and a

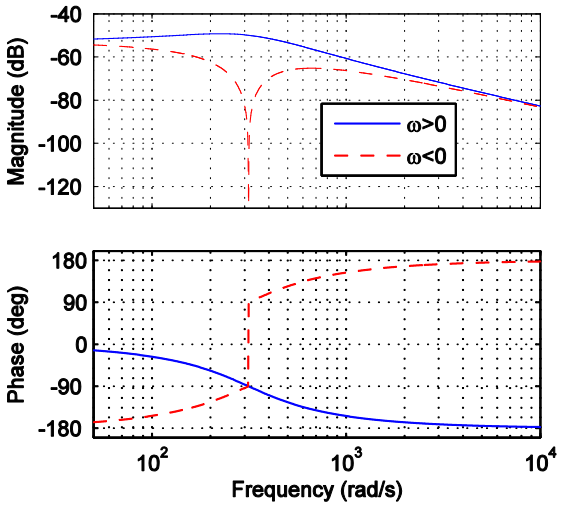

Fig. 6. Frequency response of the transfer function $\Psi_{\alpha}^{+}(s) / v_{\alpha}(s)$

notch filter behavior for the fundamental negative-sequence signal.

Without measured grid voltages, the grid VF vector $\boldsymbol{\Psi}$ can be estimated by

$$\boldsymbol{\Psi} = \int (\boldsymbol{u} + R\boldsymbol{i})dt + L\boldsymbol{i} \tag{7}$$

where R and L are the resistance and the inductance of the reactors, respectively (as shown in Fig. 1), $\boldsymbol{i}$ represents the line current vector, and $\boldsymbol{u}$ stands for the converter terminal voltage vector. In this research, the α and β components of $\boldsymbol{u}$ are calculated based on the duty cycles of modulator D_{a}, D_{b}, D_{c} and the measured DC-link voltage v_{DC} (as given by (8)).

$$u_{\alpha} = \int \left(\sqrt{\frac{2}{3}} v_{\mathrm{DC}} \left(D_{\mathrm{a}} - \frac{1}{2}(D_{\mathrm{b}} + D_{\mathrm{c}}) \right) \right) dt \tag{8a}$$

$$u_{\beta} = \int \left(\sqrt{\frac{1}{2}} v_{\mathrm{DC}} (D_{\mathrm{b}} - D_{\mathrm{c}}) \right) dt. \tag{8b}$$

Therefore, without AC voltage sensors, the fundamental sequence component of grid VF can be obtained in the $\alpha - \beta$ reference frame by combining (7)-(8) with the sequence component generation scheme shown in Fig. 5.

2.3 Power analysis in general case

As pointed out in [20], the generic instantaneous power expression can be given by

$$\begin{bmatrix} p \\ q \end{bmatrix} = \begin{bmatrix} \bar{p} + \tilde{p} \\ \bar{q} + \tilde{q} \end{bmatrix} \tag{9}$$

where $\tilde{p}$ and $\tilde{q}$ denote the oscillating parts of p and

q, while $\overline{p}$ and $\overline{q}$ are their average parts, which are represented as

$$\begin{bmatrix}\overline{p}\\ \overline{q}\end{bmatrix}=\begin{bmatrix}\sum_{n=1}^{\infty}[3V^{+n}I^{+n}\cos(\gamma^{+n}-\phi^{+n})\\ +3V^{-n}I^{-n}\cos(\gamma^{-n}-\phi^{-n})]\\ \sum_{n=1}^{\infty}[3V^{+n}I^{+n}\sin(\gamma^{+n}-\phi^{+n})\\ -3V^{-n}I^{-n}\sin(\gamma^{-n}-\phi^{-n})]\end{bmatrix} \tag{10}$$

where V^n and I^n stand for the RMS value of the n-th harmonic contained in the phase voltage and line current, respectively, with γ^n and ϕ^n for their initial phase angles.

As revealed by (10), all components contained in the voltage and the current contribute to the average active and reactive power, if only they are at the same frequency and in the same sequence (positive or negative). This conclusion can be extended to the VF based instantaneous power, i.e., the average value of VF based instantaneous power is generated from the VF and the current having the same frequency and sequence component.

2.4 Mathematical model

According to the conclusion obtained in Section 2.3 we deduce that the line current should be the fundamental positive-sequence component (i.e., balanced and sinusoidal) if the following three conditions are satisfied simultaneously, (i) $\overline{p}$, $\overline{q}$ only contain the power generated from fundamental positive-sequence components (denoted by p^+, q^+), (ii) p^+, q^+ are calculated based on fundamental positive-sequence grid signals (voltage or VF). The VF is adopted here (as given by (11)), and (iii) A controller can make the positive-sequence power p^+, q^+ track constant power references strictly.

$$\begin{bmatrix}p^+\\ q^+\end{bmatrix}=\begin{bmatrix}\omega(\Psi_\alpha^+ i_\beta-\Psi_\beta^+ i_\alpha)\\ \omega(\Psi_\alpha^+ i_\alpha+\Psi_\beta^+ i_\beta)\end{bmatrix} \tag{11}$$

Literature [21] proposed a voltage sensorless DPC for three-phase VSCs. This control strategy considered the time delay existing in a real system, and exhibited superior steady-state and transient performance. In order to facilitate the illustration of the control strategy proposed in this paper, the controller mathematical model of [21] is given as below

$$\begin{bmatrix}u_\alpha(k)\\ u_\beta(k)\end{bmatrix}=\begin{bmatrix}\hat{v}_\alpha(k)\\ \hat{v}_\beta(k)\end{bmatrix}-\frac{L}{T_s(\hat{v}_\alpha^2+\hat{v}_\beta^2)}\begin{bmatrix}\hat{v}_\alpha(k) & \hat{v}_\beta(k)\\ \hat{v}_\beta(k) & -\hat{v}_\alpha(k)\end{bmatrix}\cdot\begin{bmatrix}p_{\text{app}}^*(k+1)-p(k)\\ q_{\text{app}}^*(k+1)-q(k)\end{bmatrix} \tag{12}$$

where $\hat{v}$ denotes the estimated grid voltage, T_s represents the sampling period and p_{app}^*, q_{app}^* give the amended power reference values, which are defined as

$$\begin{aligned}\begin{bmatrix}p_{\text{app}}^*(k+1)\\ q_{\text{app}}^*(k+1)\end{bmatrix}&=\begin{bmatrix}p^*(k+1)+\eta_p\varepsilon_p(k)\\ q^*(k+1)+\eta_q\varepsilon_q(k)\end{bmatrix}\\&=\begin{bmatrix}2p^*(k)-p^*(k-1)+\eta_p[p^*(k)-p(k)]\\ 2q^*(k)-q^*(k-1)+\eta_q[q^*(k)-q(k)]\end{bmatrix}\end{aligned} \tag{13}$$

where $\eta_{p,q}$ are the delay compensation coefficients and $\varepsilon_{p,q}$ are power tracking errors. In (13), the first RHS expression p^*, q^* represent the original references, and the second RHS expression, e.g. $\eta_{p,}\varepsilon_p(k)$, is the delay compensation term.

Based on the deduction conducted in this section, (12) is rewritten as

$$\begin{bmatrix}u_\alpha(k)\\ u_\beta(k)\end{bmatrix}=\omega\begin{bmatrix}-\Psi_\beta^+(k)\\ \Psi_\alpha^+(k)\end{bmatrix}-\frac{L}{\omega T_s(\Psi_\alpha^{+2}+\Psi_\beta^{+2})}\cdot\begin{bmatrix}-\Psi_\beta^+(k) & \Psi_\alpha^+(k)\\ \Psi_\alpha^+(k) & \Psi_\beta^+(k)\end{bmatrix}\begin{bmatrix}p_{\text{app}}^*(k+1)-p^+(k)\\ q_{\text{app}}^*(k+1)-q^+(k)\end{bmatrix} \tag{14}$$

It is well known that, with a classic PI controller used in the outer DC-link voltage loop, the oscillating power cannot be thoroughly eliminated from the active power reference. To adapt the proposed SOGI-VFPDPC to this classic outer loop controller and enhance its robustness against the negative influence of an unbalanced voltage dip, the fundamental negative-sequence VF is superimposed on the converter reference voltage. Accordingly, the final controller mathematical model is given as

$$\begin{bmatrix}u_\alpha(k)\\ u_\beta(k)\end{bmatrix}=\omega\begin{bmatrix}-\Psi_\beta^+(k)+\Psi_\beta^-(k)\\ \Psi_\alpha^+(k)-\Psi_\alpha^-(k)\end{bmatrix}-\frac{L}{\omega T_s(\Psi_\alpha^{+2}+\Psi_\beta^{+2})}\cdot\begin{bmatrix}-\Psi_\beta^+(k) & \Psi_\alpha^+(k)\\ \Psi_\alpha^+(k) & \Psi_\beta^+(k)\end{bmatrix}\begin{bmatrix}p_{\text{app}}^*(k+1)-p^+(k)\\ q_{\text{app}}^*(k+1)-q^+(k)\end{bmatrix} \tag{15}$$

$$\begin{bmatrix}p_{\text{app}}^*(k+1)\\ q_{\text{app}}^*(k+1)\end{bmatrix}=\begin{bmatrix}2p^*(k)-p^*(k-1)+\eta_p[p^*(k)-p^+(k)]\\ 2q^*(k)-q^*(k-1)+\eta_q[q^*(k)-q^+(k)]\end{bmatrix} \tag{16}$$

where the fundamental sequence components of estimated grid voltages are realized by the corresponding sequence components of grid VF.

3. Simulation Results

The simulation studies have been conducted using MATLAB/Simulink and the toolbox SimPowerSystems. In order to test the performance of the proposed SOGI-

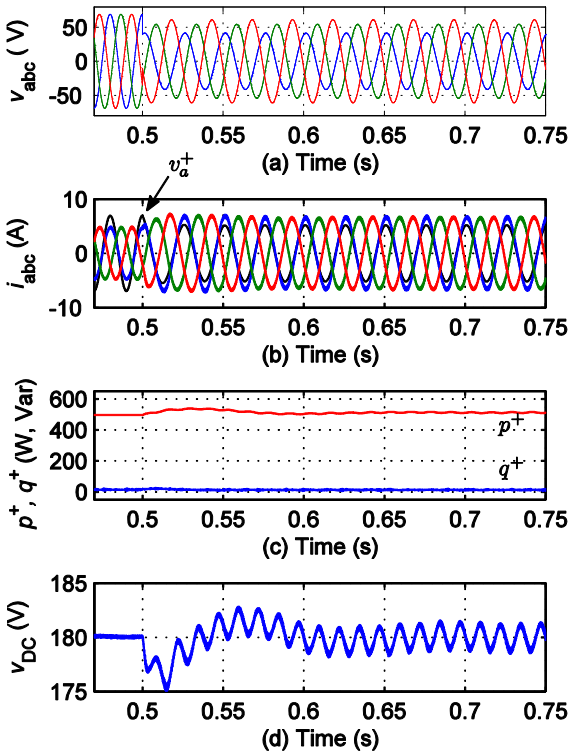

Fig. 7. Simulation results of the proposed strategy in the presence of an unbalanced voltage sag and a frequency variation from 50 to 40 Hz, $v_{DC}^{*}=180$ V and q^{*}=0 Var

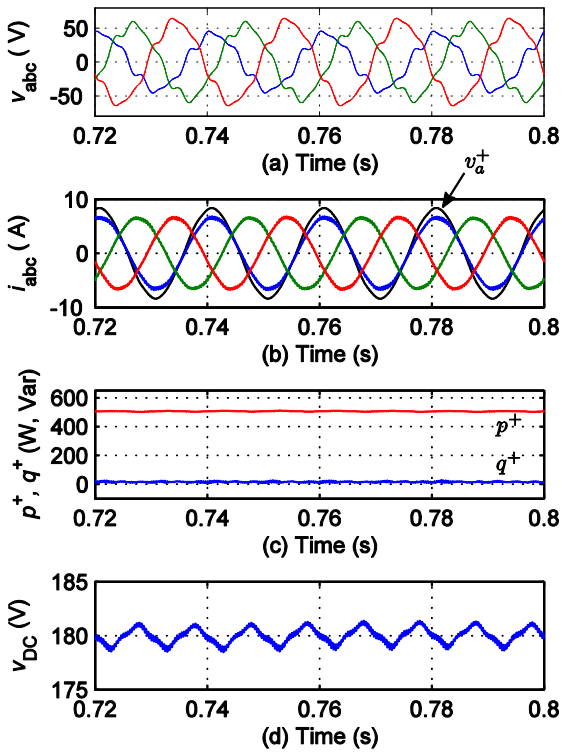

Fig. 8. Simulation results of the proposed strategy in the presence of harmonics and an unbalanced voltage sag, $v_{DC}^{*}=180$ V and q^{*}=0 Var

VFPDPC, three types of simulated grid disturbances are considered in the following simulation studies. In the first case, the grid voltage experiences a frequency deviation and an unbalanced voltage dip (involving amplitude and phase angle steps). In the second one, the negative influence of higher harmonics is added. The main parameters of the electrical circuit utilized in simulation and experimental verifications are set as: resistance of reactors $R=0.67\ \Omega$, inductance of reactors $L=19.5$ mH, DC-link capacitor $C=1120\ \mu F$, phase voltage $V_{RMS}=49.07$ V, source voltage frequency $f=$ 50 Hz, DC-link voltage $v_{DC}=180$ V, sampling period $T_s=200\ \mu$s and switching frequency $f_{sw}=5$ *k*Hz. Since the rectifier mode of VSCs is selected for the performance check, a load resistance $R_{load}=68.6\ \Omega$ is connected in the DC-link side.

Fig. 7 gives the simulation results for the proposed strategy when the grid voltage is disturbed by an unbalanced voltage dip and a frequency deviation simultaneously. As shown in Fig. 7(a), grid disturbances occur at 0.5 s. The unbalanced voltages consist of $\boldsymbol{v}^{+}=0.747\angle-14^{\circ}$ pu and $\boldsymbol{v}^{-}=0.163\angle 8.63^{\circ}$ pu, with $\boldsymbol{v}_{pf}^{+}=1\angle 0^{\circ}$ pu for the pre-fault phase voltage (49.07 V_{RMS}), and the grid frequency jumps from 50 to 40 Hz. Fig. 7(b) indicates that the line currents offered by the proposed strategy are symmetrical and sinusoidal in the steady state before and under grid disturbances, and the transient process is smooth. The total harmonic distortion (THD) generated at 50 and 40 Hz are 2.3 and 0.83%, respectively. The flat waveforms of instantaneous power shown in Fig. 7(c) also verify the aforementioned observations about line currents. Moreover, a series of simulation studies indicates, with and without fundamental negative-sequence VF feedforword, the unbalance factor (defined as I^{-}/I^{+}) of the line current are 0.62 and 1%, respectively. The unbalance factor is 0.75% when the DC-link voltage loop and the VF feedforward are both disconnected, and the active power reference is set to a constant value which makes the average DC-link voltage be 180 V. This confirms the effectiveness about unbalance regulation discussed in Section 2.4. In Fig. 7(b), the line currents are nearly in phase with the positive-sequence grid voltages. The tiny reactive power offset, reflected by Fig. 7(c), is caused by the assumption that the grid voltage is constant at adjacent sampling instants. This offset can be reduced by increasing the sampling frequency. The double frequency fluctuations appearing in the DC-link voltage (Fig. 7(d)) is caused by the interaction between line currents and the fundamental negative-sequence component of grid voltages. Nevertheless, the average DC-link voltage is kept at the reference value (180 V) after reestablishing a steady state.

Fig. 8 shows the simulation results of the proposed strategy when the higher harmonics are added to the

unbalanced voltage used in Fig. 7. The harmonics contain both $\boldsymbol{v}^{-5} = 0.07\angle -60^{\circ}$ pu and $\boldsymbol{v}^{+7} = 0.05\angle 30^{\circ}$ pu. As evidenced by Fig. 8, although the grid voltages are distorted seriously, the line currents still keep near-sinusoidal waveforms(THD=2.35% for $k = 0.7$ and 3.49% for $k = \sqrt{2}$). The above results reveal that a smaller k of QVFO can further weaken the negative influence of higher harmonics. The harmonic tolerance of the line current is due to the utilization of the fundamental positive-sequence power as the control variable and the harmonic attenuation effect offered by the sequence component generation strategy. The peak-to-peak value of DC voltage is 2.9 V, i.e., 1.61% of reference value (180 V).

Fig. 9 compares the tracking performance between the proposed strategy and the conventional PDPC proposed in [7], when a step change of the instantaneous active power reference is applied. This test is carried out under the same grid condition as that employed in Fig. 8. It can be noted from Fig. 9 that the fast dynamic response of the conventional PDPC is preserved by the proposed one. The rising time of the instantaneous active power shown in Figs. 9(a) and 9(b) are both 0.4 ms. Furthermore, Fig. 9 also indicates that the balanced sinusoidal operation is ensured by the proposed SOGI-VFPDPC before and after the reference step change, whereas the line currents of the conventional PDPC are seriously distorted all the time. The fluctuations of the line current amplitudes around 0.655 s (shown in 9(a)) are mainly caused by the grid frequency re-estimation after the step change occurrence.

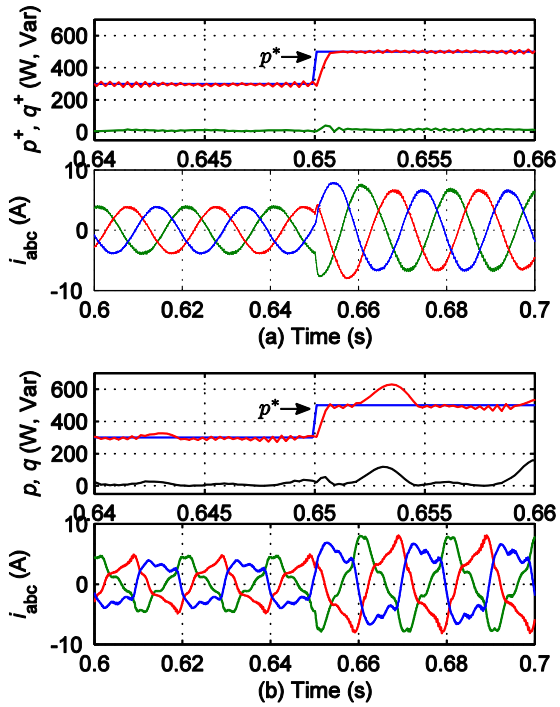

Fig. 9. Transient responses for the instantaneous active power reference p^* step change from 300 to 500 W in the presence of harmonics and an unbalanced voltage sag. (a) Proposed SOGI-VFPDPC. (b) Conventional PDPC

4. Experimental Verifications

The experimental evaluation of the proposed SOGI-VFPDPC is performed on the experimental platform shown in Fig. 10. It comprises a three-phase IGBT (SEMIKRON SKM50GB12T4) based VSC connected to a programmable AC source (CHROMA 61511). The control strategy was implemented in dSPACE 1104, and the driving signals were applied to IGBT after voltage lifting via the drivers (SEMIKRON SKYPER32R). Due to the current capability limit, the pre-fault phase-to-phase voltage is set to $V_{\text{L-L(RMS)}} = 50$ V, and the DC-link voltage reference is reduced to 80 V.

Fig. 11 gives the experimental results corresponding to the simulations in Fig. 7. In this case, the phase a, b and c voltages are set as 17.3, 22.7 and 25.5 V, respectively, to imitate the voltage dip characterized by $\boldsymbol{v}^{+} = 0.747\angle -14^{\circ}$ pu and $\boldsymbol{v}^{-} = 0.163\angle 8.63^{\circ}$ pu. Meanwhile, the grid frequency experiences a step change from 50 to 40 Hz. Fig. 11(b) reflects that the line currents are still sinusoidal (THD= 1.71%) and balanced during the unbalanced voltage dip accompanying with the grid frequency step change. In addition, there are no undesired overshoots of the line currents at the instant when the disturbance occurs. The above phenomena are well agreed with the simulation results observed in Fig. 7. Fig. 11(d) reflects that, different from Fig. 11(b), the same grid disturbance as that used in fig. 11(b) induces the line current generated by the conventional PDPC to be unbalanced and seriously distorted (the line current THDs of phase a, b and c are 12.4, 12.67 and 12.35%, respectively). Fig. 11(c) gives the steady-state results with the proposed strategy during the above grid disturbance. The actual instantaneous power p and q are also given in Fig. 11(c), which are calculated

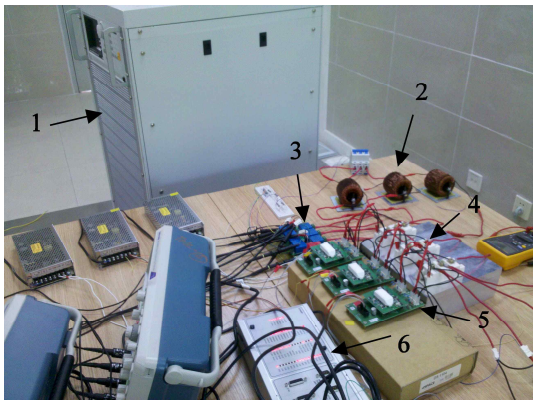

Fig. 10. Laboratory setup: 1) programable AC source, 2) reactors, 3) voltage and current sensor board, 4) voltage source converter, 5) IGBT drivers, 6) dSPACE CP1104

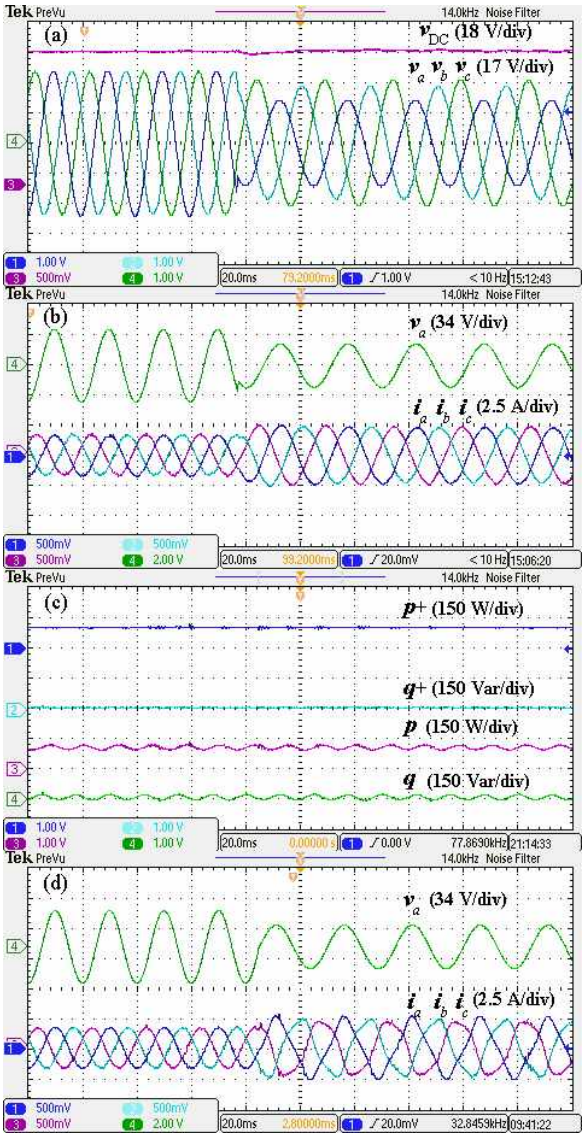

Fig. 11. Experimental results obtained when an unbalanced voltage dip and a grid frequency step occur simultaneously. (a)-(c) Proposed SOGI-VFPDPC. (d) Conventional PDPC

based on measured voltages (just used for the actual power flow illustration). The differences existing in the positive-sequence and actual power flows indicate that the balanced sinusoidal line currents are at the cost of oscillations presenting in the actual power. In this case, the power oscillations, presenting in sinusoidal waves at the double frequency, are generated by the line current and fundamental negative-sequence voltage.

Fig. 12 is devoted to evaluating the immunity of the proposed scheme to the harmonic distortion of grid voltages. In this case, the fundamental phase voltage is set to 22 V, and higher harmonics comprise 7% of the fifth harmonic and 5% of the seventh harmonic. The experimental oscillograms are shown in Fig. 12. As reflected by Fig. 12, the intentionally added higher harmonics distort the line

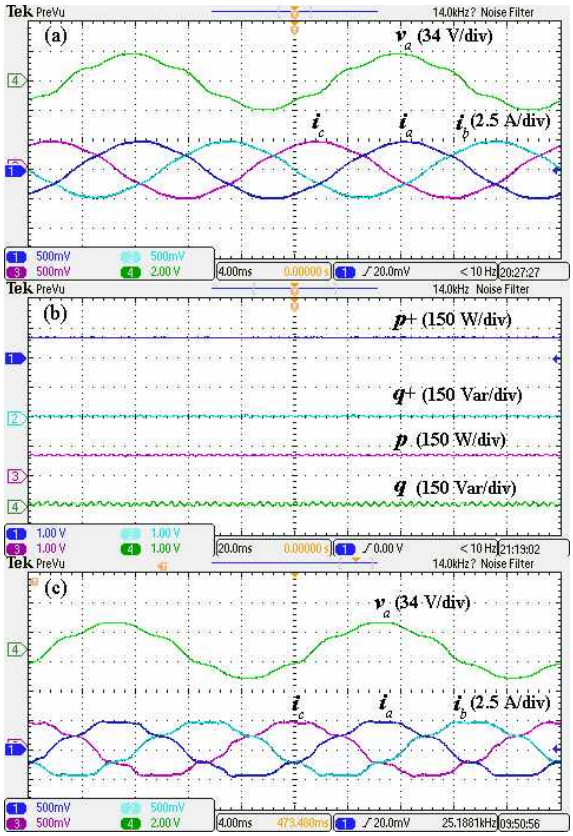

Fig. 12. Experimental oscillograms obtained under distorted grid voltages (7% of the fifth harmonic and 5% of the seventh harmonic). (a)-(b) Proposed SOGI-VFPDPC. (c) Conventional PDPC

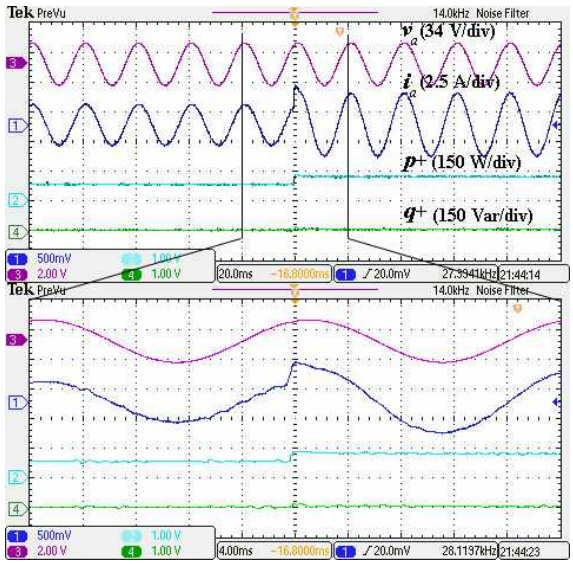

Fig. 13. Transient response of the proposed SOGI-PDPC for p^* step from 80 to 120 W under an unbalanced voltage condition

currents generated by using the conventional PDPC more severely than that offered by the proposed strategy, and the

THDs of them are 9.86 (Fig. 12(c)) and 3.75% (Fig. 12(a)), respectively. The ripples appearing on actual power curves, exhibited in Fig. 12(b), cannot be avoided due to the interaction between the generated line current and higher harmonics of the grid voltage.

The transient response of the proposed strategy for p^* step change is tested under the same unbalanced voltage dip as that used in Fig. 11, and the experimental oscillograms are given in Fig. 13. As reflected by Fig. 13, the experimental results are similar to the simulation results exhibited in Fig. 9, that is, a fast and smooth dynamic process is achieved by using the proposed strategy.

5. Conclusion

This paper has presented a SOGI-VFPDPC for grid-connected three-phase VSCs dealing with unbalanced and distorted grid conditions. By utilizing the SOGI based VF observer, the proposed SOGI-VFPDPC achieves an AC voltage sensorless operation, realizes a grid frequency adaptive control, and the hardware structure of control system is simplified. Meanwhile, the proposed strategy employs the fundamental positive-sequence active and reactive power as control variables to perform the unbalance regulation and the harmonic suppression of line currents. The waveform control of line currents is also contributed by using the fundamental negative-sequence VF feedforward and the QVFO-based sequence component generation. Simulation and experimental results demonstrate that the proposed strategy can achieve balanced sinusoidal line currents independent of unbalanced voltage dip, grid frequency deviation and higher harmonic distortion. Moreover, it can also be observed from the experimental results that oscillations appear in actual power flows. That is inevitable due to the interaction between the generated balanced sinusoidal line currents and the fundamental negative-sequence component or harmonics of the grid voltage. From comparison studies, it can be concluded that the proposed SOGI-VFPCPC offers an excellent steady-state performance, which cannot be met by the conventional PDPC, while preserving the fast transient response performance of the conventional one.

Acknowledgements

The work was supported by Guangdong Innovative Research Team Program (No. 201001N0104744201) and Doctoral Scientific Research Foundation of Zhengzhou University of Light Industry.

References

[1] Y. Suh, Y. G, and D. Rho, "A comparative study on control algorithm for active front-end rectifier of large motor drives under unbalanced input," *IEEE Trans. Ind. Applicat.*, vol. 47, no. 3, pp. 1419-1431, May/Jun.2011.

[2] F. Blaabjerg, Z. Chen, and S. B. Kjaer, "Power electronics as efficient interface in dispersed power generation systems," *IEEE Trans. Power Electron.*, vol. 19, no. 5, pp. 1184-1194, Sep. 2004.

[3] B. A. Welchko, T. A. Lipo, T. M. Jahns, and S. E. Schulz, "Fault tolerant three-phase AC motor drive topologies: A comparision of features, cost, and limitations," *IEEE Trans. Power Electron.*, vol. 19, no. 4, pp. 1108-1116, Jul. 2004

[4] *Standard for interconnecting distributed resources with electric power systems*, IEEE Std. 1547-2003, Sep. 2010.

[5] A. Timbus, M. Liserre, R. Teodorescu, P. Rodriguez, and F. Blaabjerg, "Evaluation of current controllers for distributed power generation systems," *IEEE Trans. Power Electron.,* vol. 24, no. 3, pp. 654-664, Mar. 2009.

[6] T. Noguchi, H. Tomiki, S. Kondo, and I. Takahashi, "Direct power control of PWM converter without power-source voltage sensors," *IEEE Trans. Ind. Applicat.*, vol. 34, no. 3, pp. 473-479, May/Jun. 1998.

[7] A. Bouafia, J. P. Gaubert, and F. Krim, "Predictive direct power control of three-phase pulsewidth modulation (PWM) rectifier using space-vector modulation (SVM)," *IEEE Trans. Power Electron.*, vol. 25, no. 1, pp. 228-236, Jan. 2010.

[8] P. Cortes, J. Rodriguez, P. Antoniewicz, and M. Kazmierkowski, "Direct power control of an AFE using predictive control," *IEEE Trans. Power Electron.*, vol. 23, no. 5, pp. 2516-2523, Sep. 2008.

[9] M. Malinowski, M. Jasinski, and M. P. Kazmierkowski, "Simple direct power control of three-phase PWM rectifier using space-vector modulation (DPC-SVM)," *IEEE Trans. Ind. Electron.*, vol. 51, no. 2, pp. 447-454, Apr. 2004.

[10] K. Ma, W. Chen, M. Liserre, and F. Blaabjerg, "Power controllability of a three-phase converter with an unbalanced AC source," *IEEE Trans. Power Electron.*, vol. 30, no. 3, pp. 1591-1604, Mar. 2015.

[11] L. Shang and J. Hu, "Sliding-mode-based direct power control of grid-connected wind-turbine-driven doubly fed induction generators under unbalanced grid voltage conditions," *IEEE Trans. Energy Convers.*, vol. 27, no. 2, pp. 362-373, Jun. 2012.

[12] J. Hu and Z. Q. Zhu, "Investigation on switching patterns of direct power control strategies for grid-connected DC-AC converters based on power variation rates," *IEEE Trans. Power Electron.*, vol. 26, no. 12, pp. 3582-3598, Dec. 2011.

[13] M. Malinowski, G. Marques, M. Cichowlas, and M. P. Kazmierkowski, "New direct power control of three-phase pwm boost rectifiers under distorted and

imbalanced line voltage conditions," in *Proc. IEEE ISIE*, vol. 1, Jun. 2003, pp. 438-443.
[14] M. P. Kazmierkowski, M. Jasinski, and G. Wrona, "DSP-based control of grid-connected power converters operating under grid distortions," *IEEE Trans. Ind. Electron.*, vol. 7, no. 2, pp. 204-211, May 2011.
[15] P. R. Martinez-Rodriguez, G. Escobar, A. A. Valdez-Fernandez, M. Hernandez-Gomez, and J. M. SosaE, "Direct power control of a three-phase rectifier based on positive sequence detection," *IEEE Trans. Ind. Electron.*, vol. 61, no. 8, pp. 4084-4092, Aug. 2014.
[16] J. A. Suul and T. Undeland, "Impact of virtual flux reference frame orientation on voltage source inverters in weak grids," in *Proc. IPEC*, Sapporo, Jun. 2010, pp. 468-375.
[17] N. R. N. Idris and A. H. M. Yatim, "An improved stator flux estimation in steady-state operation for direct torque control of induction machines," *IEEE Trans. Ind. Appl.*, vol. 38, no. 1, pp. 110-116, Jan./Feb. 2002.
[18] A. Kulka, "Sensorless digital control of grid connected three phase converters for renewable sources," Ph.D. dissertation, Norwegian Univ. Sci. Technol., Trondheim, Norway, 2009.
[19] J. A. Suul, A. Luna, P.Rodriguez, and T. Undeland, "Voltage-sensor-less synchronization to unbalanced grids by frequency-adaptive virtual flux estimation," *IEEE Trans. Ind. Electron.*, vol. 59, no. 7, pp. 2910-2923, Jul. 2012.
[20] H. Akagi, E.Watanabe, and M.Aredes, *Instantaneous Power Theory and Applications to Power Conditioning*. New York: Wiley, 2007.
[21] Y. K. Tao, Q. H. Wu, L. Wang, and W. H. Tang, "Voltage sensorless predictive direct power control of three-phase PWM converters," *IET Power Electron.*, vol. 9, no. 5, pp. 1009-1018, Apr. 2016.

Yukun Tao received the M.Eng. degree from the Department of Electrical Engineering and Automation, Henan Polytechnic University, Jiaozuo, China, in 2011, and the Ph.D. degree from the School of Electric Power Engineering, South China University of Technology, Guangzhou, China, in 2016. Currently, he is a Lecturer in the School of Electrical and Information Engineering, Zhengzhou University of Light Industry, Zhengzhou, China. His research interests are mainly related to analysis and control of power electronic converters and renewable energy integration in power grids.

Wenhu Tang (M'05-SM'13) received the B.Eng. and M.Sc. degrees in electrical engineering from Huazhong University of Science and Technology, Wuhan, China, in 1996 and 2000, respectively, and the Ph.D. degree in electrical engineering from The University of Liverpool, Liverpool, U.K., in 2004. He was a Postdoctoral Research Associate and subsequently a Lecturer at The University of Liverpool between 2004 and 2013. He is currently a Distinguished Professor and the Vice Dean of the School of Electric Power Engineering, South China University of Technology, Guangzhou, China. He has authored and coauthored more than 100 research papers, including 40 journal papers and 1 Springer research monograph. His research interests include renewable energy integration in power grids, condition monitoring and fault diagnosis for power apparatus, multiple-criteria evaluation, and intelligent decision support systems.